Numerical study of a foam-shock trap based blast mitigation strategy

S. S. Prasanna Kumar, K. Ramamurthi, and B. S. V. Patnaik

Citation: Physics of Fluids **30**, 086102 (2018); doi: 10.1063/1.5043177
View online: https://doi.org/10.1063/1.5043177
View Table of Contents: http://aip.scitation.org/toc/phf/30/8
Published by the American Institute of Physics

Numerical study of a foam-shock trap based blast mitigation strategy

S. S. Prasanna Kumar,[1] K. Ramamurthi,[2] and B. S. V. Patnaik[1,a)]
[1]*Department of Applied Mechanics, Indian Institute of Technology Madras, Chennai 600036, India*
[2]*Department of Mechanical Engineering, Indian Institute of Technology, Chennai 600036, India*

(Received 6 June 2018; accepted 11 August 2018; published online 28 August 2018)

Blast mitigation using various types of foams is of interest to practitioners for the safe design of structures. Experimental and numerical studies have demonstrated the beneficial effects of different foam materials when used as protective soft coatings. However, under certain blast loading conditions and foam dimensions, the load experienced by the target/protected structure was found to be much higher in the presence of foam than in its absence. In this study, a mechanism based on geometric means known as shock trap is used along with foam as a preventive measure against shock amplification. A shock trap is a special arrangement of rigid obstacles with an air gap, designed to offer a tortuous flow path. To analyze the proposed foam-shock trap combination, a popular Lagrangian based Smoothed Particle Hydrodynamics (SPH) is employed. A novel solid wall boundary modeling technique called skew gradient wall boundary treatment is also built into the SPH solver. The material discontinuity is handled by a multimass correction strategy. The blast wave mitigation characteristics of the proposed approach are evaluated using two different foam materials, namely, wet aqueous foam and polystyrene foam. From detailed simulations, it was observed that undesirable shock enhancement effect of foams was found to be completely suppressed by combining it with the shock trap mechanism. The proposed foam shock trap combination significantly reduces the peak load and impulse experienced by the target structure. *Published by AIP Publishing.* https://doi.org/10.1063/1.5043177

I. INTRODUCTION

Blast waves have a detrimental influence on structures and their mitigation is of practical interest. A comprehensive review of the blast mitigation methods can be found in the work of Igra *et al.*[1] and Britan *et al.*[2] Most Blast Wave Mitigation (BWM) strategies either employ deformable protective layers that dissipate/absorb energy or tend to reflect the wave. In the former class of methods, studies have shown that foam based barrier structures are highly effective in attenuating shocks.[3–8] In particular, aqueous foams[3,9,10] and polymer based foams such as polyether foam,[11] polyurethane foam,[4] polyethylene foam,[12] polystyrene,[13] etc., have gained prominence. In general, foams have attractive attributes such as (i) light weight, (ii) high strength to weight ratio, (iii) low cost and ready availability, (iv) tailorable material properties such as density, porosity, etc., (v) superior energy absorption capability, etc. However, in a number of experiments it was observed that, under some conditions, foams are counterproductive to their original objective as they cause *shock enhancement or amplification* of the loads. Under certain test conditions, the load exerted was found to be much higher than the value measured without the layer of foam. In the context of blast protection using foams, this effect is highly undesirable and is typically found in configurations which allow free compaction of the foam material against the protected structure. Although the dynamical processes leading to this effect are not completely understood, studies have shown that shock amplification can be avoided by increasing the thickness of the foam material beyond a certain critical value. A comprehensive review of the various studies that reported this effect can be found in the work of Zhu *et al.*[14]

In foam-based approaches, the predominant mode of attenuation is through an *absorptive mechanism*, in which the incident energy of the blast wave is dissipated through plastic deformation. This is different from the use of water wall,[15] concrete wall,[16] perforated plates,[17] steel meshes,[18] array of rigid obstacles,[19,20] etc. which redirect the energy of the blast wave away from the protected structure, exemplifying the *reflective mechanism* of blast mitigation. Among these approaches, a particular method known as shock-trapping, introduced by Skews *et al.*,[21] is of interest in the present study. A specific arrangement of wedge shaped obstacles placed along the path of the shock wave facilitates a less resistive entry than the exit. The flow path past these obstacles is designed such that stronger reflection coupled with vortex generation dissipates the energy of the blast wave. Later, Chaudhuri *et al.*[22] have suggested an improved shock trap by modifying the arrangement, which in turn provided better attenuation of shock waves.

In the present study, we first simulate the conditions for which the foam mitigates the blast wave. The reflected shock from the restricted motion of the rear surface of the foam or compaction as it were is necessary to be dissipated for adequate mitigation and is explored with using shock traps. We thereafter investigate the effectiveness of using a combination of foam and shock trap in protecting the target structure. In particular, we study the influence of shock trap setup on the shock enhancement effect due to foam compaction. The analyses are carried out numerically using Smoothed Particle Hydrodynamics (SPH) simulations. The outline of the paper

a)Electronic mail: bsvp@iitm.ac.in

is as follows: in Sec. II, the governing SPH equations are presented, along with the solution algorithm and the material model used for different foams. In Sec. III, the validation studies are presented. The problem domain with initial and boundary conditions is described in Sec. IV. The results of the simulations are discussed in Sec. V. Finally, the paper ends with a brief summary and conclusions.

II. GOVERNING EQUATIONS AND METHOD OF SOLUTION

The propagation of waves in different medium can be described using the unsteady, inviscid, conservation equations (1),

$$\frac{D\rho}{Dt} = -\rho\nabla\cdot\mathbf{v}, \tag{1a}$$

$$\frac{D\mathbf{v}}{Dt} = -\frac{\nabla p}{\rho}, \tag{1b}$$

$$\frac{Du}{Dt} = -\frac{p}{\rho}\nabla\cdot\mathbf{v}. \tag{1c}$$

Here, $\frac{D}{Dt}$ is the material derivative and ρ, p, u, and $\mathbf{v}$ represents the density, pressure, specific internal energy, and velocity vector, respectively.

A. SPH equations of motion

SPH is a mesh-free, Lagrangian, particle based numerical framework used for solving a wide range of engineering problems.[23] In the SPH methodology, the discrete form of the governing PDEs is obtained using either the variational principles or kernel interpolation theory. The former is always preferred as it provides a set of equations which is unique, Galilean invariant, and, in particular, conservative. A detailed derivation and discussion of the SPH theory can be found in Refs. 24 and 25. For the present study, the discretised equations of motion are as follows:

$$\rho_i = \frac{m_i}{V_i}, \quad V_i = \frac{1}{\sum_j W_{ij}(r_{ij},h_i)}, \tag{2}$$

$$\frac{D\mathbf{v}_i}{Dt} = -\frac{1}{m_i}\sum_j\left(\frac{p_j V_j^2}{\tilde{\Omega}_j}\nabla_i W\left(r_{ij},h_j\right) + \frac{p_i V_i^2}{\tilde{\Omega}_i}\nabla_i W\left(r_{ij},h_i\right)\right), \tag{3}$$

$$\frac{Du_i}{Dt} = \frac{p_i}{\rho_i^2}\frac{m_i}{\tilde{\Omega}}\sum_j \mathbf{v}_{ij}\cdot\nabla_i W\left(r_{ij},h_j\right). \tag{4}$$

In the above equation, m, V, and h denote the mass, volume, and smoothing length of the particles, respectively, W is the kernel function, r_{ij} is the inter-particle distance, $\nabla_i W_{ij}$ is the gradient of the kernel function, and $\tilde{\Omega}_i$ is a *correction* term accounting for the adaptive smoothing length defined as follows:

$$\tilde{\Omega}_i \equiv 1 - m_i\frac{\partial h_i}{\partial\rho_i}\sum_j\frac{\partial W(h_i)}{\partial h}. \tag{5}$$

An artificial viscosity term (6) is added to the discrete form of the momentum equation (3), to ensure proper resolution of shocks in compressible flow simulations. The artificial viscosity term prevents inter-particle penetration in the case of high speed, convergent flows and also serves to suppress any non-physical noise in the solution,

$$\dot{\mathbf{v}}_{diss,i} = \sum\frac{m_j}{\bar{\rho}_{ij}}\bar{\alpha}_{ij}v_{ij}^{sig,v}\mathbf{v}_{ij}\cdot\hat{\mathbf{x}}_{ij}\overline{\nabla_i W_{ij}}, \tag{6}$$

$$v_{ij}^{sig,v} = \begin{cases} 0.5(c_i + c_j - \beta\mathbf{v}_{ij}\cdot\hat{\mathbf{x}}_{ij}) & if\ \mathbf{v}_{ij}\cdot\hat{\mathbf{x}}_{ij} < 0 \\ 0 & otherwise. \end{cases} \tag{7}$$

In Eq. (6), α is a variable coefficient that controls the amount of dissipation, $v^{sig,v}$ is the signal velocity calculated based on the sound speed (c) and relative velocity of an interacting particle pair, and $\overline{\nabla_i W_{ij}}$ represents the arithmetic average $0.5\left\{\nabla_i W(r_{ij},h_i) + \nabla_i W(r_{ij},h_j)\right\}$. The additional parameter β is set as 2.0 following the work of Price.[26] Any quantity, say, velocity $\mathbf{v}_{ij}$ represents $\left(\mathbf{v}_i - \mathbf{v}_j\right)$ and the quantity $\bar{\mathbf{v}}_{ij}$ represents the average $0.5\left(\mathbf{v}_i + \mathbf{v}_j\right)$. Similar notation applies for other variables.

For compressible flows involving large viscous heating, the artificial heat conduction term [the second term in Eq. (8)] is added to the thermal energy evolution equation. For the current study, we use the form proposed by Price[26] as follows:

$$\dot{u}_{diss,i} = \sum_j\frac{m_j}{\bar{\rho}_{ij}}\left\{-0.5\bar{\alpha}_{ij}v_{ij}^{sig,v}\left(\mathbf{v}_{ij}\cdot\hat{\mathbf{x}}_{ij}\right)^2 + \bar{\kappa}_{ij}u_{ij}v_{ij}^{sig,u}\right\}\hat{\mathbf{x}}_{ij}\cdot\overline{\nabla_i W_{ij}}. \tag{8}$$

In Eq. (8), κ is a control parameter and $v^{sig,u}$ is the signal velocity defined as $v_{ij}^{sig,u} = \sqrt{\frac{|p_{ij}|}{\bar{\rho}_{ij}}}$.

It should be pointed out that the artificial viscosity and conductivity terms are required only in the shocked regions. To achieve this selective usage, the technique introduced by Cullen and Dehnen[28] is implemented to adapt the control parameters α and κ. The particle's value of α is set as

$$\alpha_{loc,i} = \alpha_{max}\frac{h_i^2 A_i}{h_i^2 A_i + \epsilon_\alpha v_{sig,i}^2}, \tag{9}$$

where A_i is calculated as

$$A_i = \zeta_i\max\left(-\dot{\nabla}\cdot\mathbf{v}_i, 0\right) \tag{10}$$

and the signal velocity $v_{sig,i}$ is calculated as

$$v_{sig,i} = \max_{|\mathbf{x}_{ij}|\le h_i}\left(\bar{c}_{ij} - \min\left(0, \mathbf{v}_{ij}.\hat{\mathbf{x}}_{ij}\right)\right). \tag{11}$$

If $\alpha_{loc,i}$ is higher than the particle's previous value, then $\alpha_{loc,i}$ is set as the α_i. Otherwise, α is relaxed as follows:

$$\dot{\alpha}_i = \frac{\alpha_{loc,i} - \alpha_i}{\tau_i}, \quad \tau_i = \frac{h_i}{0.05 v_{sig,i}}. \tag{12}$$

For the present simulations, α_{max} is set as 2.5 based on the benchmark problems presented by Cullen and Dehnen[28] for strong shocks. The limiter quantity ζ is required to reduce false detection (see Ref. 27 for more details). To limit the action of artificial heat conductivity around regions of jump discontinuity, an approach similar to the artificial viscosity is followed for adapting the value of κ as

$$\kappa_{loc,i} = \kappa_{max}\frac{h_i^2 A_i}{h_i^2 A_i + \epsilon_\kappa v_{sig,i}^2}, \tag{13}$$

where

$$A_i = \max\left\{\frac{-R_i|\dot{\nabla}u_i|}{\sqrt{u_i}}, 0\right\}, \quad |\dot{\nabla}u_i| = \frac{|\nabla u_i|^n - |\nabla u_i|^{n-1}}{\Delta t}. \quad (14)$$

If the value of $\kappa_{loc,i}$ is less than its previous value, it is relaxed according to

$$\dot{\kappa}_i = \frac{\kappa_{loc,i} - \kappa_i}{\tau_i} \quad , \quad \tau_i = \frac{h_i}{0.05 v_{sig,i}}. \quad (15)$$

Appropriate Equations of State (EoS) for different materials are presented under material modeling.

B. Material modeling

1. Air

Air is assumed to be a perfect gas with the adiabatic index $\gamma_a = 1.4$. The equation of state is

$$p_a = (\gamma_a - 1)\rho_a u_a. \quad (16)$$

Setting $\rho_0 = 1$ kg/m^3 and $p_0 = 1 \times 10^5$ Pa, the value of specific acoustic impedance $z_0 = \rho_0 c_0$ for air is 374.16 Pa s/m. Here, subscript "0" denotes the values at standard ambient conditions.

2. Explosive products

The gaseous products of an explosive material are modeled using the Jones-Wilkins-Lee Equation of State (JWL-EoS) as follows:

$$p = A\left(1 - \frac{\omega v}{r_1}\right)\exp\left(\frac{-r_1}{v}\right) + B\left(1 - \frac{\omega v}{r_2}\right)\exp\left(\frac{-r_2}{v}\right) + \omega v \rho_e u, \quad ; \quad v = \frac{\rho}{\rho_e}, \quad (17)$$

where A, B, r_1, r_2, and ω are the constants depending on the type of explosive employed, ρ_e and E_0 are the density and energy of the un-reacted explosive, respectively, and D is the detonation velocity. The JWL-EoS parameters for pentolite is presented in Table I. The detonation process of the explosive is modeled using the programmed burn algorithm.[29]

3. Foamed polystyrene

In the present study, an equation of state (18) based on the stiffened gas approach, proposed by Sugiyama *et al.*,[13] is used for modeling polystyrene foam,

$$p = (\gamma_s - 1)\rho u - \gamma_s b. \quad (18)$$

In Eq. (18), the value of γ_s and b is set as 1.8 and 2.07×10^6, respectively.[13] The values of density and acoustic speed for the polystyrene foam are $\rho_f = 35$ kg/m^3 and $c_f = 336.9$ m/s, respectively,[13] and therefore, its specific acoustic impedance is 1.18×10^4 Pa s/m.

4. Wet aqueous foam

For modeling wet aqueous foams, the pseudo-gas approach used by Sembian *et al.*[3] is followed. Assuming foam to be a homogeneous mixture of air and water, the density of the foam is calculated based on the rule of mixtures as

$$\rho_f = (1 - \alpha_f)\rho_a + \alpha_f \rho_w, \quad (19)$$

where ρ_f, ρ_w, and ρ_a denote the density of foam, water, and air, respectively, and α_f is the volume fraction defined as

$$\alpha_f = \frac{V_w}{V_a + V_w}. \quad (20)$$

Here, V_w and V_a denote the volume of water and air in the foam, respectively. The pressure of the foam particles is calculated using the Nobel-Abel equation of state,

$$p_f = \frac{(\gamma_f - 1)\rho_f u_f}{1 - \alpha_f}. \quad (21)$$

In Eq. (21), the specific heat ratio for the foam (γ_f) is obtained as

$$\frac{1}{\gamma_f - 1} = \frac{\alpha_f}{\gamma_w - 1} + \frac{1 - \alpha_f}{\gamma_a - 1}. \quad (22)$$

Setting $\alpha = 0.1$, $\rho_{water} = 1000$ kg/m^3, $\rho_{air} = 1$ kg/m^3, $\gamma_{water} = 7$, and $\gamma_{air} = 1.4$, we get $\rho_f = 100.9$ kg/m^3 and $\gamma_f = 1.44$. With acoustic speed in the aqueous foam $c_f = 36$ m/s, the specific acoustic impedance value is 3.63×10^3 Pa s/m.

C. Material interface treatment

Numerical analysis of foam-based BWM using the SPH methodology requires multimass particle setup (particles of different materials have different values of mass). However, the existing SPH formulations suffer from numerical errors around the contact discontinuities (CD) due to the multimass particle setup. Therefore, a multimass correction procedure proposed by Prasanna Kumar *et al.*[30] is implemented to accurately resolve the material interfaces. The exchange of mass between particles across the mass discontinuity line is determined through

$$\dot{m}_{diff,i} = \sum_j \frac{\overline{m}_{ij}}{\overline{\rho}_{ij}} \psi_{ij} v_{ij}^{sig,m} m_{ij} \hat{\mathbf{x}}_{ij} \cdot \overline{\nabla_i W_{ij}}, \quad (23)$$

where

$$v_{ij}^{sig,m} = \begin{cases} \sqrt{\frac{|p_{ij}|}{\bar{\rho}_{ij}}} & \text{if } \mathbf{v}_{ij} \cdot \hat{\mathbf{x}}_{ij} < 0 \\ 0 & \text{otherwise.} \end{cases} \quad (24)$$

The quantity ψ_{ij} is a limiter function to regulate the amount of diffusion. Using the right value of ψ_{ij} is crucial as higher values can lead to over correction and erroneous results. For all the simulations, ψ_{ij} was calculated as follows:

$$\psi_{ij} = \frac{(\mathbf{v}_{ij} \cdot \hat{\mathbf{x}}_{ij})^2}{\mathbf{v}_{ij} \cdot \mathbf{v}_{ij} + (\epsilon_\psi v_{ij}^{sig,m})^2 + (0.001\bar{c}_{ij})^2}. \quad (25)$$

TABLE I. JWL-EoS parameters for the gaseous products of pentolite are taken from Ref. 13.

Explosive	A	B	r_1	r_2	ω	ρ_e (kg/m^3)	E_0	D (m/s)
Pentolite	531.77×10^9	8.933×10^9	4.6	1.05	0.33	1650	4.85×10^6	7500

The limiter itself can be further tuned using ϵ_ψ. For the present study, the value of ϵ_ψ is set as 0.1. Allowing mass diffusion of the particles necessitates that the following additional correction terms should be added to restore momentum and energy conservation:

$$\dot{\mathbf{v}}_{diss,i} = \frac{1}{m_i}\sum_j Q_{ij} m_{ij} \mathbf{v}_j, \tag{26}$$

$$\dot{u}_{diss,i} = \frac{1}{m_i}\sum_j Q_{ij} m_{ij} \left\{0.5\left(\mathbf{v}_j \cdot \mathbf{v}_j\right) + u_j\right\}. \tag{27}$$

Here, $Q_{ij} = \psi_{ij}\frac{\overline{m}_{ij}}{\overline{\rho}_{ij}} v_{ij}^{sig,m} \hat{\mathbf{x}}_{ij} \cdot \overline{\nabla_i W_{ij}}$.

D. Imposing boundary conditions

In this section, the inflow, outflow, and wall boundary models used in the present study are briefly described.

1. Inflow/outflow boundary modeling

In SPH, permeable boundaries are modeled by constructing a buffer zone with particles along the direction of outward normal to the boundary. The size of the buffer zone is chosen such that a full compact support is available for the fluid particles near the boundaries. As soon as the buffer particles cross the inlet, they are flagged as fluid particles which are then evolved as governed by the conservation equations. As the fluid particles cross the outlet, they are flagged as buffer particles. In the inlet buffer zone, new buffer particles are continuously replenished as older buffer particles are transformed into fluid particles. The physical properties of the particles in the buffer zone are suitably assigned to enforce the required boundary conditions.

2. Wall boundary treatment

In the present study, we employ the skew gradient Wall Boundary Treatment (sgWBT) method proposed by Prasanna Kumar *et al.*[20] for imposing the conditions at the wall boundaries. The procedure begins with the calculation of the properties of wall particles by taking the kernel average from the fluid particles within its support domain. For a generic fluid property A, the kernel average is obtained as follows:

$$\tilde{A}_w = \frac{\sum_{j\in f} A_j W(r_{jw}, h_w)}{\sum_{j\in f} W(r_{jw}, h_w)}, \tag{28}$$

where subscript w and f denote a wall and fluid particle, respectively. The properties of the virtual particles are then assigned by extrapolating the value of the nearest wall particle using Taylor series expansion. This requires that the local gradient at the wall particles be calculated using the following equation:

$$\nabla A_w = \sum_j \frac{m_j}{\rho_j}(A_j - A_{nf})\nabla W^s. \tag{29}$$

In (29), subscript nf denotes the nearest fluid particle in the vicinity of the wall particle under consideration and $\nabla W^s(\mathbf{R}')$ is the gradient of a skewed kernel function.[31] The skew gradient of a chosen symmetric kernel function (W) can be calculated as

$$\nabla W^s(\mathbf{R}') = \nabla W(|\mathbf{R}'|)\left[1 + erf\left(\boldsymbol{\lambda}\cdot\mathbf{R}'\right)\right] + \frac{2\boldsymbol{\lambda} W}{h\sqrt{\pi}}\exp\left\{-(\boldsymbol{\lambda}\cdot\mathbf{R}')^2\right\}, \tag{30}$$

where $\mathbf{R}' = \frac{\mathbf{x}'-\mathbf{x}}{h}$ and $\boldsymbol{\lambda}$ is the skewness vector. The skewness vectors for the wall particles are set as $\boldsymbol{\lambda}_w = -c\hat{\mathbf{n}}^w$. Here, $\hat{\mathbf{n}}^w$ is the wall normal vector (see Fig. 1) and c is a suitable constant (set as 10 in the present study) which controls the quantum of skewness. Finally, the properties of the virtual particles are assigned using the following equation:

$$A_{vir}(\mathbf{x}) = \tilde{A}_{nw}(\mathbf{x}') + \Delta\mathbf{x}\cdot\nabla A|_{nw}, \tag{31}$$

where subscript nw denotes the nearest wall particle and $\Delta\mathbf{x} = (\mathbf{x} - \mathbf{x}')$.

E. Time integration scheme

The time integration of the equations is carried out using a 2nd order accurate predictor-corrector scheme. The time evolution of any quantity $\mathbf{a}$ is obtained as follows:
Predictor step:

$$\mathbf{a}_i^{n+\frac{1}{2}} = \mathbf{a}_i^n + \frac{\Delta t}{2}\left.\frac{d\mathbf{a}_i}{dt}\right|^n. \tag{32}$$

Corrector step:

$$\mathbf{a}_i^{n+\frac{1}{2}} = \mathbf{a}_i^n + \frac{\Delta t}{2}\left.\frac{d\mathbf{a}_i}{dt}\right|^{n+\frac{1}{2}}, \tag{33}$$

$$\mathbf{a}_i^{n+1} = 2\mathbf{a}_i^{n+\frac{1}{2}} - \mathbf{a}_i^n, \tag{34}$$

where $n, n+\frac{1}{2}$, and $n+1$ represents the present, intermediate, and subsequent time level, respectively. A variable time step size determined by the Courant-Friedrichs-Lewy (CFL) criterion given in (35) is used for time marching,

$$\Delta t = 0.25 \min_{1\le i\le N}\left\{\frac{h_i}{||\mathbf{v}_i|| + c_i}\right\}. \tag{35}$$

Here, N is the total number of particles in the domain.

F. Other numerical details

To ensure sufficient neighbour particles for the calculations, the value of the smoothing length (h) is adapted according to particle density (which depends on the local inter-particle spacing). The coupled variables (ρ and h) are therefore

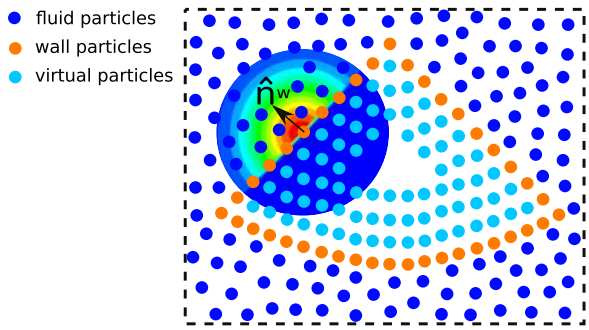

FIG. 1. Schematic of wall boundary modeling using the sgWBT method.

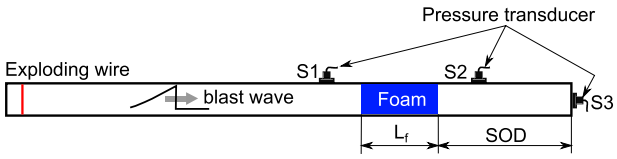

FIG. 2. Schematic of the experiment conducted by Sembian *et al.*[3]

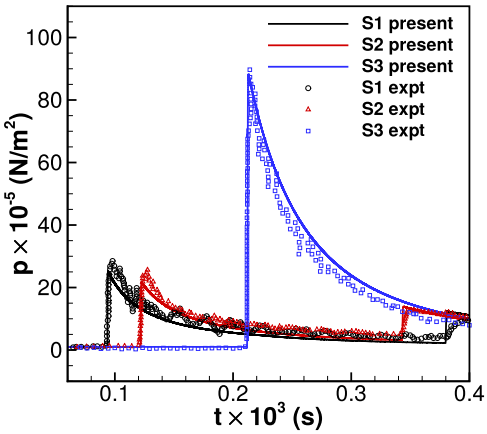

FIG. 3. Numerical validation of the aqueous foam model. Comparison of temporal variation of pressure at different spatial locations S1, S2, and S3 against the experimental measurement.

calculated using the bisection method with convergence criteria set as $|\frac{h^{k+1}-h^k}{h_{initial}}| < 10^{-2}$. For assigning smoothing length, we choose the relation $h = \eta V^{\frac{1}{d}}$, where V is the particle volume and d is the number of dimensions. Wendland $W_{3,3}$ kernel[32] with a support size $H = 4\Delta x$ is used in the present study to avoid pairing instability[27] and for improved accuracy.[33] The solver was developed in C++ with a double precision storage. To speed up the calculations, the particles' neighbour search was conducted using a linked-list algorithm and code parallelisation was carried out using OpenMP libraries.

III. VALIDATION STUDIES

In this section, the results of the numerical simulations employing various material models are validated.

A. Validation of aqueous foam model

The aqueous foam experiments conducted by Sembian *et al.*[3] are simulated using the present numerical model. The schematic of the apparatus is depicted in Fig. 2. The experimental setup is a long, uniform cross-sectioned tunnel, with an exploding wire at one end to generate the blast wave. The aqueous foam to be tested was placed at a standoff distance (*SOD*) from the other end-wall of the tunnel fitted with a pressure sensor. Additional sensors were flush mounted at different locations along the length of the tunnel to monitor the temporal variation of pressure. A one dimensional computational domain of length 0.358 m was discretised into a total of 5200 SPH particles. Reflective boundary conditions were applied at both ends of the domain. To start with, the initial conditions for the numerical simulation of exploding wire were determined using a trial and error approach. The initial conditions around the point of explosion was tuned, until the cumulative least square error from the three pressure sensor locations [190 mm (*S*1), 234 mm (*S*2), and 358 mm (*S*3) from the left end of the tunnel] matched within 5% of the experiments. The initial conditions so obtained are

$$(p, \rho, u) = \begin{cases} (1030 \times 10^5, 95.82, 0) & \text{for } 1 \le x \le 3 \\ (1.01 \times 10^5, 1.17, 0) & \text{for } x \le 1 \text{ and for } x \ge 3 \end{cases}. \tag{36}$$

A comparison of the pressure history obtained from the numerical simulations against the experimental data is presented in Fig. 3.

To validate the foam model, the foam particles were positioned at a zero standoff distance from the *S*3 location. Then, using the aforementioned initial conditions, the time of arrival (t_a) of the blast wave at the *S*3 location was obtained for different values of foam thickness (L_f). From Fig. 4(a), a fairly good agreement between the numerical and experimental values for the time of arrival can be observed. Additionally, the numerically obtained temporal variation of pressure at the *S*3 location, corresponding to a foam thickness of 2 cm and a standoff distance of 8 cm, is compared against the experimental measurement in Fig. 4(b). An excellent match between the two indicates the ability of the model to accurately predict the interaction between the blast wave and the aqueous foam.

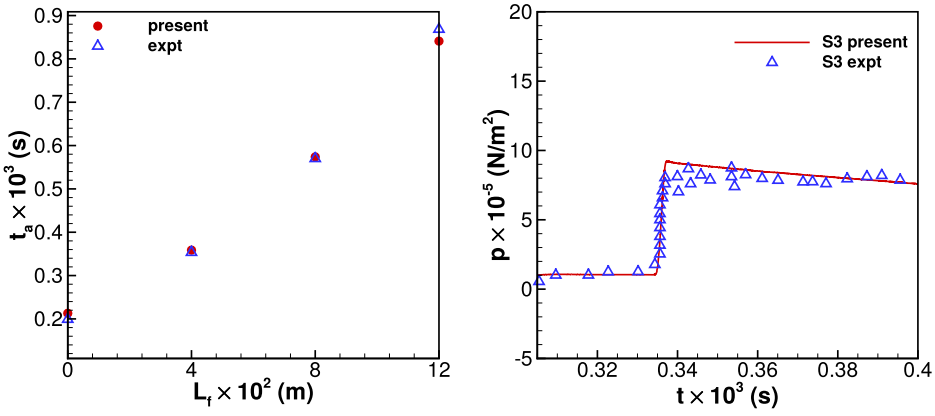

FIG. 4. Numerical validation of the aqueous foam model: (a) Comparison of the predicted time of arrival of the blast wave at *S*3 location against the experimental measurement for different values of foam thickness. (b) Comparison of the predicted temporal variation of pressure at *S*3 location against the experimental measurement for the case of L_f = 2 cm and *SOD* = 8 cm.

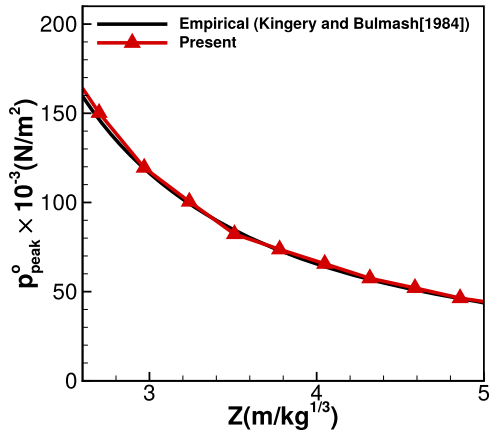

FIG. 5. Comparison of the predicted peak overpressure against the empirical relation proposed by Kingery and Bulmash.[37]

B. Validation of polystyrene foam model

An experimental study on blast mitigation using the polystyrene foam was carried out by Homae *et al.*[34] Subsequently, the results of their experiment were used by Sugiyama *et al.*[13] for the development and validation of a 2D, axisymmetric, Harten-Lax-van Leer (HLL)/Harten-Lax-van Leer-Contact (HLLC) scheme based solver. In their numerical formulation, Sugiyama *et al.*[13] have proposed a stiffened gas approach to model the polystyrene foam which is carefully followed in setting up the problem domain for the present study. A spherically shaped pentolite charge of radius 0.024 m and 0.1 kg in mass is covered by a layer of polystyrene foam of radius 0.076 m. The charge is detonated in a quiescent atmosphere under standard, sea level, ambient conditions. The schematic of the computational domain is shown in Fig. 6(a). To validate the material model for the polystyrene foam, an axisymmetric SPH formulation was required. In the present work, an axisymmetric SPH scheme proposed by Brookshaw[35] along with the improvements suggested by Garcia-Senz *et al.*[36] is implemented. The relevant 2D, axisymmetric, SPH equations of motion can be found in Ref. 36. For simulating the process of detonating the charge, a simple, programmed burn model[29] is followed.

To ensure that the axisymmetric formulation of the SPH solver and the detonation model are sufficiently accurate, the standard hemispherical surface free-field air blast problem is simulated, for which empirical relations are available. For this test, we consider the explosion of a pentolite charge of mass 0.1 kg in standard sea level ambient condition. The variation of peak overpressure (p^o_{peak}) with the corrected scaled distance (Z) is plotted in Fig. 5. The simulation results can be seen to be in excellent agreement with the empirical relation proposed by Kingery and Bulmash.[37]

For the validation of the polystyrene foam model, we choose a 2D computational domain of size $(0, 2.5) \times (0, 2.5)$. The domain was discretised with approximately 6.7×10^5 particles arranged in a square lattice. The explosive and the foam material were arranged as shown in Fig. 6(a). The temporal variation of the overpressure was monitored at three spatial locations (K = 3, 4, and 5) and compared against the experimental and numerical results reported by Homae *et al.*[34] and Sugiyama *et al.*[13] Figure 6 depicts a reasonably good agreement between the numerical and experimental overpressure history.

IV. BLAST MITIGATION STRATEGY USING FOAM-SHOCK TRAP COMBINATION

The blast mitigation characteristics of foams and rigid obstacles have mostly been studied individually but not together. However, when they are combined, they might exhibit different mitigation characteristics, and to be precise, the foam based blast mitigation approach facilitates an absorptive mechanism, whereas the rigid obstacles subscribe to the reflective mechanism. Therefore, the present study systematically explores their combined influence on the overall blast mitigation.

In the case of foams, the energy extraction from the incident blast wave is achieved through plastic deformation. Although, this mechanism seems intuitively efficient, the simple impedance mismatch at the foam-air and air-foam interfaces can play a significant role in modifying the incident blast wave parameters. This realisation has, in fact, led to the study of functionally graded materials.[38,39] In the case of non-graded foam materials, significantly higher mitigation is achievable by simply providing a separation or standoff distance (SOD) between the foam and the protected structure[40] (which exploits the impedance mismatch at the foam-air interface). To this end, we propose a shock trap to avoid the foam compaction against the protected structure and the attendant shock amplification effects.

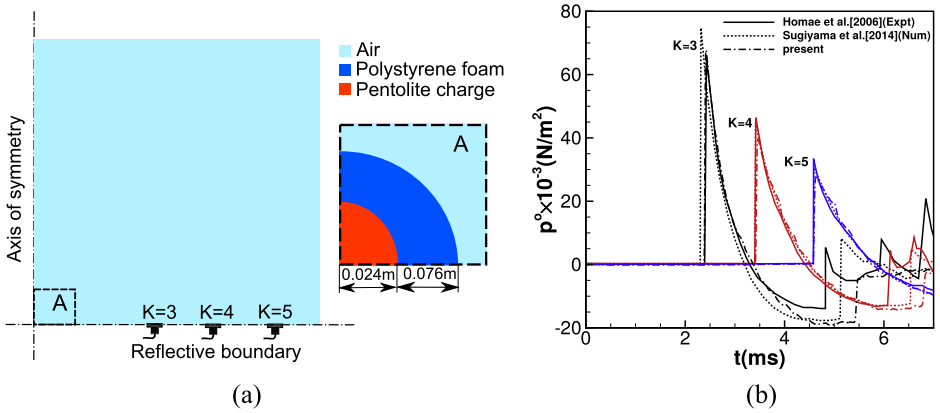

FIG. 6. (a) Schematic of the problem domain for validation of the polystyrene foam model. (b) Comparison of the temporal variation of overpressure against the experimental results of Homae *et al.*[34] and the numerical results of Sugiyama *et al.*[13]

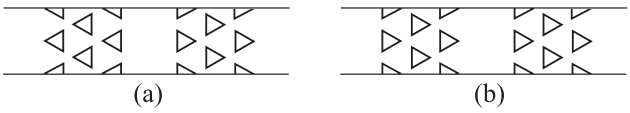

FIG. 7. (a) Schematic of the shock trap proposed by Skews *et al.* (b) Schematic of the improved version of the shock trap proposed by Chaudhuri *et al.*

A typical schematic of a shock trap is shown in Fig. 7(a). The shock trap consists of two sets of obstacle arrays separated by a short gap. Each obstacle array is made up of multiple columns of wedge-shaped obstacles in a staggered arrangement. The cross section of the obstacles allows relatively easy entrance to the air gap region compared to the exit. Once the incident shock enters the trap region, it undergoes several reflections before emerging as a weaker transmitted wave. These obstacles not only redirect the flow in the lateral directions but also promote flow non-uniformity through the generation of vortices. The interaction of the waves in the trap region with these vortices enhances the flow disturbances. Eventually, the flow becomes turbulent and much of the kinetic energy is dissipated by the eddies. In a numerical study carried out by Chaudhuri *et al.*,[22] a modified arrangement of the obstacle was shown to provide even better attenuation levels. The schematic of the modified obstacle arrangement is shown in Fig. 7(b). Assuming that the incident shock or blast wave always travels from left to right, the direction in which the first set of obstacles are pointing was reversed. Unlike the original, the modified configuration resulted in an increased resistance to flow, with a stronger shock reflection at the entrance. The results have shown that the transmitted shock is considerably weaker for the modified arrangement. Hence, in the present simulations, the modified arrangement is investigated for its ability to mitigate shock amplification effect.

A. Problem domain

The interaction of a blast wave with a foam-shock trap combination is an inherently three dimensional, multicomponent, compressible fluid flow problem with complex boundary conditions. Immense computational resources are required to simulate this problem in its totality. Therefore, suitable assumptions are applied to reduce its complexity. For the ease of simulation, we assume the shock trap to be an array of vertically aligned rigid rods with uniform cross section, placed ahead of the target structure. A layer of foam material with uniform cross section is positioned at the entrance of the shock trap. A planar blast wave is assumed to enter the computational domain through the left boundary as shown (see Fig. 8). The aforementioned assumptions reduce the problem to two dimensions owing to planar symmetry. However, it is pointed out that modeling three dimensional effects such as the deformation of the fluid/material interfaces[41] and complex shock interface interaction[42,43] is essential for more accurate quantification of possible mitigation levels. The schematic of the problem domain is depicted in Fig. 8. Assuming the actual height of the target structure to be much greater than the length of the domain (L), the top and bottom boundaries are considered to be periodic. The length and height of the domain (H) is taken as 1.0 m and 0.12 m, respectively. The standoff distance (*SOD*) defined as the separation between the protected structure and the last array of obstacle was set as 0.17 m. The length of the air gap zone in the shock trap was chosen as 0.08 m. Assuming the target structure to be a rigid wall, the extreme right boundary of the domain is modeled using reflective boundary conditions given as

$$\frac{\partial p}{\partial x} = \frac{\partial \rho}{\partial x} = \frac{\partial u}{\partial x} = 0, \mathbf{v} = 0. \tag{37}$$

The blast wave is modeled using Eqs. (38)–(40), for the pressure, density, and velocity, respectively. They constitute the inflow boundary conditions on the left side of the domain,

$$p^o(t) = p^o_{peak}\left(1 - \frac{t}{t_+}\right)\exp\left(\frac{-\alpha t}{t_+}\right). \tag{38}$$

In Eq. (38), p^o is the over pressure defined as $p^o = p - p_0$, with p_0 being the atmospheric pressure, p^o_{peak} is the peak overpressure, t_+ is the time duration of positive overpressure, and α is the decay constant. Following Peng *et al.*,[44] the temporal variation of density and fluid velocity is obtained as follows:

$$\rho(t) = \frac{(\gamma+1)p^o(t) + 2\gamma p_0}{(\gamma-1)p^o(t) + 2\gamma p_0}, \tag{39}$$

$$v_x(t) = \sqrt{\frac{2}{\gamma p_0}}\frac{a_0 p^o(t)}{\sqrt{(\gamma+1)p^o(t) + 2\gamma p_0}}. \tag{40}$$

Here, a_0 and γ denote the ambient sound speed and adiabatic index, respectively. For the simulations in this study, we set $\frac{p^o_{peak}}{p_0} = 100.924$, $t_+ = 0.5 \times 10^{-3}$ s, and $\alpha = 2.72$. For the chosen blast wave profile, the value of the co-efficient of reflection (C_R) and shock Mach number (M_s) is approximately 7.6 and 9.4, respectively. A total of 1.23×10^6 particles were

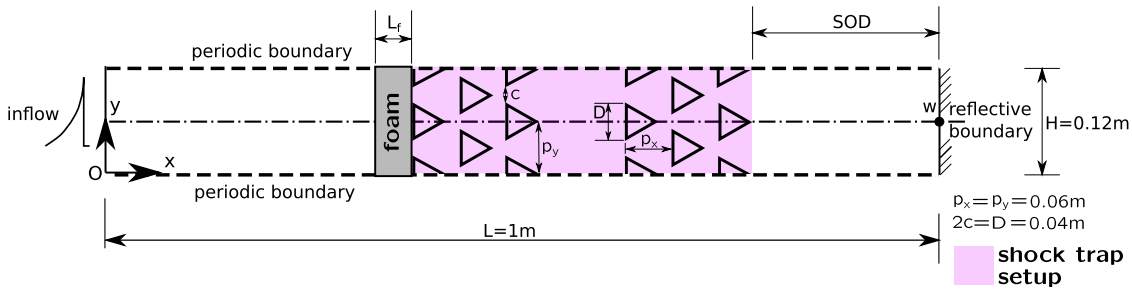

FIG. 8. Schematic of the problem domain depicting the foam-shock trap setup. Inflow boundary presents a blast wave entering the domain. Top and bottom boundaries are periodic (shown dashed). The first maze of obstacles are padded with a foam of thickness L_f. The *SOD* is measured from the end of the second set of obstacle maze.

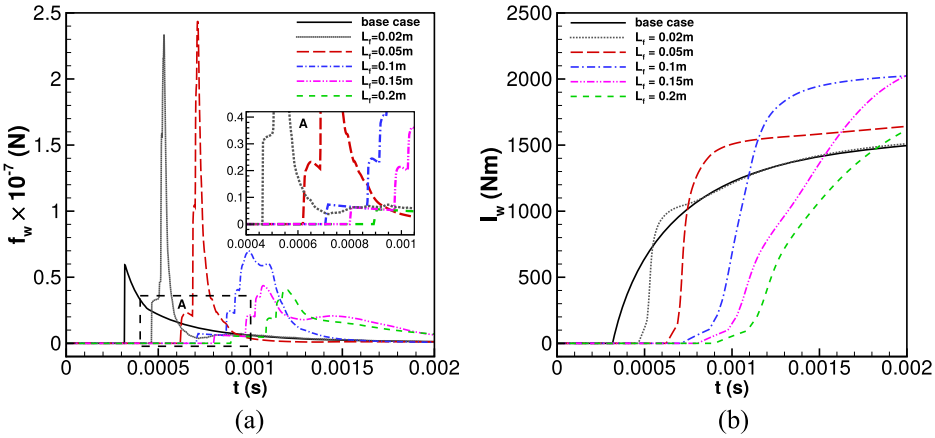

FIG. 9. Temporal variation of (a) wall force and (b) wall impulse, when the aqueous foam barrier alone is placed in the shock path. The results corresponding to different values of foam thickness (L_f) are compared against the base case.

employed for the simulation which includes the air, foam, wall, and inflow particles. The initial spacing between the particles was set as 4×10^{-4} m. The simulation with foam but without the shock trap is first carried out followed by the foam and shock trap. The simulations for the shock trap have been carried out using SPH and are presented in Ref. 20.

V. RESULTS AND DISCUSSION

A. Shock enhancement

To emphasize the effect of shock enhancement or amplification, we present the result of the simulations without the shock trap and with foam. A layer of aqueous foam was placed at a distance of 0.57 m from the protected structure. The effect of aqueous foam on the incident blast wave was examined by monitoring the total force per unit width $f_w = \int_0^H (p(y) - p_0)dy$ exerted on the structure. This analysis was carried out for different foam thickness values, L_f = 0.02 m, 0.05 m, 0.1 m, 0.15 m, and 0.2 m. A simulation without the foam material was also performed to quantify the unobstructed interaction of the blast wave with the structure (indicated as the "base case").

The temporal variation of the wall force f_w for different cases under investigation is presented in Fig. 9. The value of peak force corresponding to the base case is approximately 5.9×10^6 N. The presence of foam ahead of the structure is expected to lower this value. Yet, for the case of L_f = 0.02 m and 0.05 m, we observe that the peak force value (f_w^{max}) recorded is around 2.4×10^7 N, which is a fivefold increase, in comparison with the base case. On closer inspection, one can notice a steep rise in the magnitude of force occurring in multiple jumps. The first jump in the value of force (f_w^I) of magnitude 2.3×10^6 N occurs at time $t \approx 0.6$ ms and corresponds to the reflection of the transmitted wave at the foam-air interface. This indicates that the foam attenuated the blast wave in its path. However, the unobstructed motion of the foam toward the structure resulted in a strong densification or compaction, increasing the force on the wall by a factor of 12 (with respect to f_w^I corresponding to L_f = 0.05 m).

Similar observations could be made from the results corresponding to higher values of foam thickness. The peak wall force for L_f = 0.1 m, 0.15 m, and 0.2 m was approximately 7×10^6 N, 4.3×10^6 N, and 4.0×10^6 N, respectively. However, the value of f_w^I was as low as 7.2×10^5 N, 6.3×10^5 N, and 5.6×10^5 N, respectively. The peak force due to shock amplification can be observed to reduce with an increase in foam thickness. For an increase in the foam thickness from 0.05 m to 0.1 m and further to 0.2 m, the value of f_w^{max} has reduced by 70.8% and 83.3% (with respect to f_w^{max} corresponding to L_f = 0.05 m), respectively, and the value of f_w^I has reduced by 69.5% and 78.2% (with respect to f_w^I corresponding to L_f = 0.05 m), respectively. Although the peak force is drastically reduced, the value of f_w^I is found to be less affected by the increase in foam thickness. This implies that increasing the foam thickness alone is not an effective way to improve attenuation. Moreover, the mitigation effects of the foam is almost completely offset by the foam compaction effects resulting in a poorer overall performance. The temporal variation of impulse transmitted to the protected structure ($I_w = \int_0^t (p(t) - p_0)dt$) is shown in Fig. 9(b). Except for L_f = 0.02 m case, it is observed that the impulse transmission corresponding to different foam thickness values is higher than the base case. Although the arrival of shock corresponding to different foam thickness is delayed by twice the value of the base case, the compaction of the foam against the wall causes the impulse transmitted to reach a value that is comparable to or higher than the base case.

The variation of non-dimensioned f_w^{max}, f_w^I, and $I_w^{0.002s}$ (the impulse value corresponding to t = 2 ms) values with foam thickness is shown in Fig. 10. These quantities are

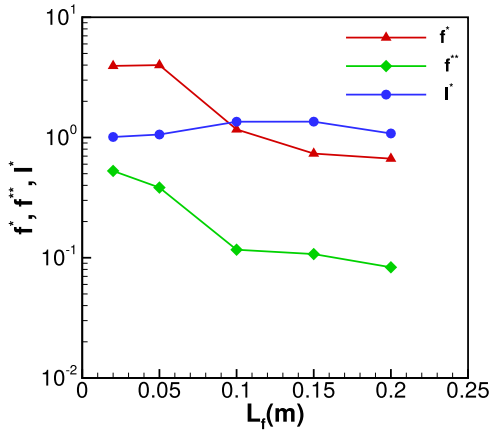

FIG. 10. Comparison of the normalised value of f_w^{max}, f_w^I, and $I_w^{t=0.002s}$ for different values of foam thickness.

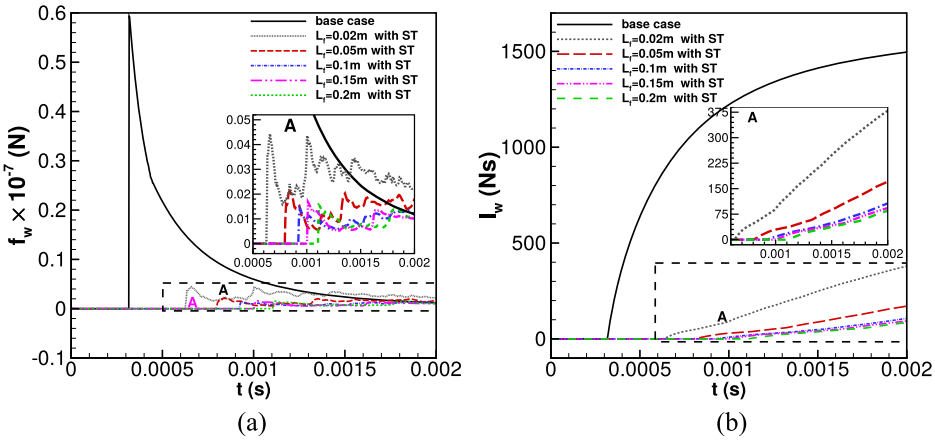

FIG. 11. Performance of the aqueous foam-shock trap setup. Temporal variation of (a) force and (b) impulse exerted on the protected structure for different foam thickness values.

normalised with the values corresponding to the base case. The non-dimensioned variables are defined as

$$f^* = \frac{f_w^{max}}{f_{w,L_f=0}^{max}}, \quad f^{**} = \frac{f_w^I}{f_{w,L_f=0}^{max}}, \quad I^* = \frac{I_w^{0.002s}}{I_{w,L_f=0}^{0.002s}}.$$

From this figure, it could be observed that increasing the foam thickness does not substantially improve the attenuation characteristics of the foam beyond $L_f = 0.1$ m (see variation of f^{**} in Fig. 10). Moreover, the values of f^* due to foam compaction is always an order of magnitude higher than its corresponding f^{**}. In summary, it is found that protection through soft coatings such as foams cannot be used in isolation.

B. Performance of aqueous foam-shock trap combination

In Sec. V A, the undesirable shock amplification effect associated with foams was demonstrated. Although a considerable wave attenuation occurs when the shock exits the foam-air interface, the unrestrained motion of the foam material and subsequent impact against the target structure impart considerably higher loads. To overcome this, rigid obstacles forming a trap is arranged between the foam and the structure. The performance of this setup under strong blast conditions is analyzed with an aqueous foam material. The blast wave parameters and the foam-shock trap setup are the same as described in Sec. IV A. The effect of foam thickness on the BWM characteristics of the aqueous foam-shock trap setup was studied by setting $L_f = 0.02$ m, 0.05 m, 0.1 m, 0.15 m, and 0.2 m.

The temporal variation of the wall force and impulse for different values of foam thickness is presented in Fig. 11. The value of peak force can be observed to be drastically reduced. For $L_f = 0.02$ m, 0.05 m, 0.1 m, 0.15 m, and 0.2 m, the corresponding value of $f_w^{max} = 4.4 \times 10^5$ N, 2.1×10^5 N, 1.4×10^5 N, 1.6×10^5 N, and 1.5×10^5 N, respectively. A closeup view of the wall force history is shown in the inset of Fig. 11(a). The second peak and fluctuations observed in the force history correspond to the multiple wave(s) reflections between the shock trap and the protected structure. Although the initial shock arrival time increases with an increase in foam thickness, the value of f_w^{max} is found to be less affected. In comparison with the base case, the reduction in peak force obtained through the aqueous foam-shock trap combination is greater than 95% for all values of foam thickness. The temporal variation of the impulse transmitted is presented in Fig. 11(b). The value of wall impulse at time $t = 0.0002$ s ($I_w^{0.002s}$ N s) is approximately 1500 N s for the base case, whereas for the aqueous foam-shock trap combination, this value is reduced by an order to approximately 150 N s. From these results, it is clearly evident that the undesirable shock amplification phenomenon has been completely eliminated with the use of the shock trap device.

To further illustrate the effectiveness of the proposed blast mitigation strategy, the performance of its individual components is compared in Fig. 12, for a foam thickness value of $L_f = 0.1$ m. While the foam barrier is found to be the least preferred approach (due to the associated shock enhancement effects), the combined foam-shock trap approach is clearly seen to be the most desirable BWM strategy. The optimised shock trap without the foam can also be seen to be quite effective, with its peak force f_w^{max} comparable to that of $f_{w,L_f=0.1\text{ms}}^I$. In this regard, the present shock trap setup and the aqueous foam material have somewhat similar mitigation potential, although their attenuation mechanisms are completely different. Table II provides a quantitative comparison of various approaches presented in Fig. 12.

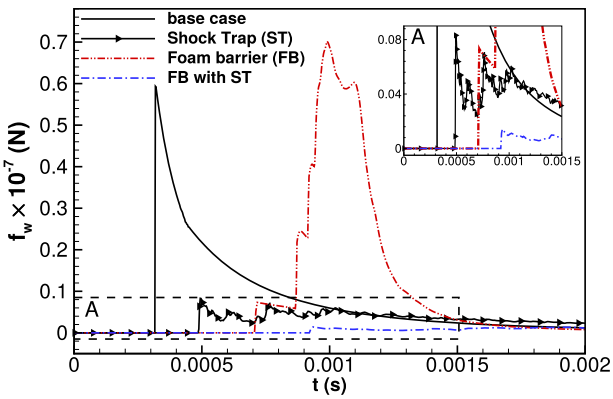

FIG. 12. Performance of the aqueous foam-shock trap setup. Comparison of the temporal variation of force for foam thickness $L_f = 0.1$ m with different mitigation approaches.

TABLE II. Effect of the aqueous foam-shock trap combination on the parameters of practical interest. The value corresponds to a foam thickness of 0.1 m.

Mitigation approach	$t_w^a \times 10^3$ (s)	$f_w^{max} \times 10^{-7}$ (N)	$f_w^I \times 10^{-7}$ (N)	$I_w^{0.002}$ (N s)
Unprotected	0.315	0.595	NA	1495.2
Aqueous foam barrier	0.706	0.702	0.073	2023.2
Shock trap	0.485	0.083	NA	579.62
Aqueous foam with shock trap	0.921	0.014	NA	106.07

The force and impulse variations for the foam and shock trap combination have clearly shown that the shock amplification effects due to foam compaction have been completely suppressed. This is primarily achieved by trapping the foam material ahead of the target structure, using the shock trap setup. To quantify this trapping effect, the amount of foam material exiting the trap is monitored. The temporal variation of the volume of foam defined as $\bar{V}_f = \frac{n_f V_p^0}{V_f^0}$ is plotted in Fig. 13(b). Here, n_f is the number of particles exiting the trap, V_p^0 is the foam particle volume at time $t = 0$ s, and V_f^0 is the total foam volume at time $t = 0$ s. For different values of foam thickness, the volume of foam that crossed the trap remain well below 10% of the initial volume, over the entire span of the simulation. This is particularly encouraging given the strong nature of the incident blast wave. For $L_f = 0.1$ m, the spatial distribution of the foam and air medium at different time instants is shown in Fig. 14, where effective containment of foam within the shock trap can be noticed.

C. Performance of polystyrene foam-shock trap combination

In this section, the blast mitigation characteristics of the polystyrene foam-shock trap setup under the strong blast conditions are presented. For the simulations, the blast wave parameters and the obstacle geometry are as given in Sec. IV A. The thickness of the polystyrene foam was varied as $L_f = 0.02$ m, 0.05 m, 0.1 m, 0.15 m, and 0.2 m. The temporal variation of the wall force and impulse are shown in Figs. 15(a) and 15(b), respectively. It can be noticed that the proposed mitigation strategy reduces the value of force and impulse transmitted to the protected structure. Except for the case of $L_f = 0.02$ m and 0.05 m, the results of other foam thickness values are comparable. The peak force value for different cases simulated is approximately 0.02×10^{-7} N. Compared to a value of 0.6×10^{-7} N, which corresponds to the base case, reduction in the peak wall force is greater than 93% for the polystyrene foam-shock trap combination. Similarly, the impulse reduction exceeds 79% for different foam thickness values that were studied.

Figure 16 demonstrates the ability of foam-shock trap combination in the effective control of undesirable shock enhancement. When a polystyrene foam barrier (case marked as FB) of thickness 0.1 m is employed, the peak wall force is amplified to a value of 2.53 times the base case. For the same foam thickness, the foam barrier with the shock trap reduces the peak wall force value to approximately 0.03 times the base case. This clearly depicts the efficacy of the proposed foam-shock trap approach in preventing the shock enhancement effect. A quantitative comparison of other relevant

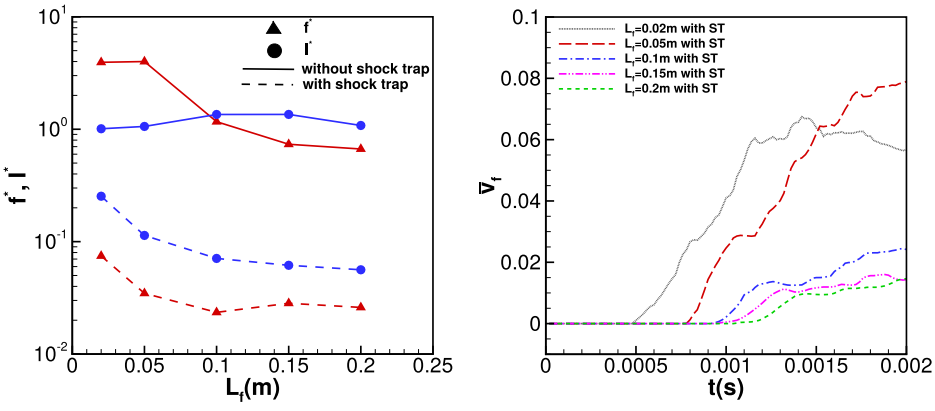

FIG. 13. Performance of the aqueous foam-shock trap setup. (a) Comparison of the peak force and impulse values (non-dimensioned using the values of the base case) for different foam thickness values. (b) Temporal variation of volume of aqueous foam exiting the shock trap.

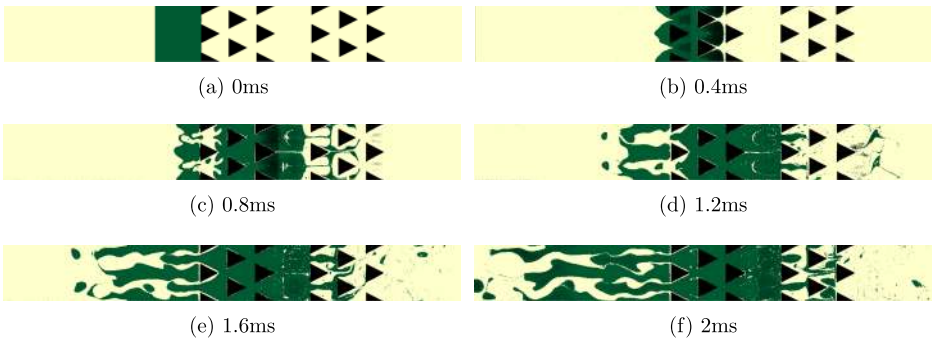

FIG. 14. Spatial distribution of air and aqueous foam medium at various time instants for $L_f = 0.1$ m case. The colour code is yellow for air and green for aqueous foam.

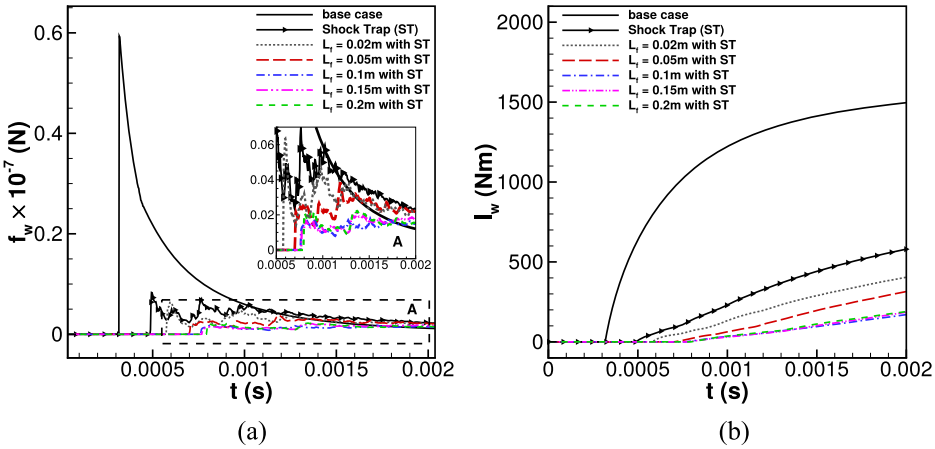

FIG. 15. Performance of the polystyrene foam-shock trap setup. Comparison of the (a) wall force and (b) impulse for different foam thickness values.

parameters for different approaches is presented in Table III. Notice a large reduction in the force and impulse transmitted and an increase in the shock arrival time for the case of foam-shock trap setup.

The variation of the non-dimensional peak wall force (f_w^{max}) and impulse ($I_w^{0.002s}$) value as a function of foam is shown in Fig. 17(a). For comparison, the values obtained without the shock trap is also shown. With the shock trap, the peak force and impulse values for the different values of L_f studied are found to be at least an order less than the case without the shock trap. While the peak force values show marginal variation with the foam thickness, the value of impulse transmitted remains almost constant. A small increase in the peak force value can be noticed in the case of $L_f = 0.2$ m. This is attributed to the reduced distance between the air-foam interface and the inflow boundary which causes a relatively higher peak pressure to be experienced by the air-foam interface when compared to lower foam thickness values (see Fig. 8). The temporal variation of the non-dimensional foam volume exiting the shock trap is shown in Fig. 17(b). For $L_f = 0.02$ m and 0.05 m case, the foam volume exiting the trap is approximately 11% and 15%, respectively, and for the remaining higher foam thickness cases, the value is less than 5% of the initial volume. As most of the foam material is blocked by the shock trap, the compaction of the foam against the protected structure and the subsequent rise in the wall force are thus prevented.

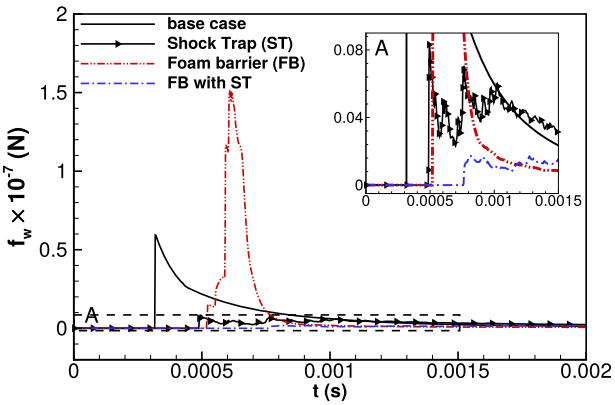

FIG. 16. Temporal variation of the wall force obtained through various setups is compared. The results correspond to a foam thickness value of 0.1 m.

Figure 18 presents a spatial distribution of the polystyrene foam and air ahead of the wall for $L_f = 0.1$ m case. Notice that due to strong blast conditions, the polystyrene foam completely disintegrates. However, the shock trap effectively prevents the foam from crossing the trapped region and thereby avoids the undesirable shock amplification effects.

D. BWM using different foams: A comparative study

In this section, the blast attenuation achieved by the aqueous foam and the polystyrene foam in combination with the shock trap is compared. It is pointed out that the density of the simulated polystyrene foam and the aqueous foam is 35 kg/m^3 and 100.9 kg/m^3, respectively. Based on relatively lower acoustic speed, lower acoustic transmission ratio at the foam-air interface, and thermal quenching effects, the aqueous foam can be argued to provide better blast attenuation. However, one of the practical difficulties of using aqueous foam is the material degradation/subsidence with time. For example, draining of liquid due to gravity (particularly in wet foams), bubble coalescence, and inter-bubble diffusion of gas lead to intrinsic dynamical variation of foam properties with time.[45] The effect of liquid drainage on the shock wave attenuation characteristics of an aqueous foam is discussed by Britan *et al.*[46] On the other hand, the polymer based foams have stable material properties and therefore are ideal as a blast mitigation device for non-contact explosion. Given that the aqueous and the polystyrene foams have vastly different properties, it would be interesting to compare their blast mitigation capabilities in conjunction with the shock trap mechanism.

Figures 19(a) and 19(b) compare the temporal variation of wall force and impulse obtained using the aqueous foam and

TABLE III. Effect of polystyrene foam-shock trap combination on the parameters of practical interest. The value corresponds to a foam thickness of 0.1 m.

Mitigation approach	$t_w^a \times 10^3$ (s)	$f_w^{max} \times 10^{-7}$ (N)	$f_w^I \times 10^{-7}$ (N)	$I_w^{0.002}$ (N s)
Unprotected	0.315	0.595	NA	1495.2
Polystyrene foam barrier	0.518	1.5	0.15	1550.5
Shock trap	0.485	0.083	NA	579.62
Polystyrene foam with shock trap	0.757	0.017	NA	170.01

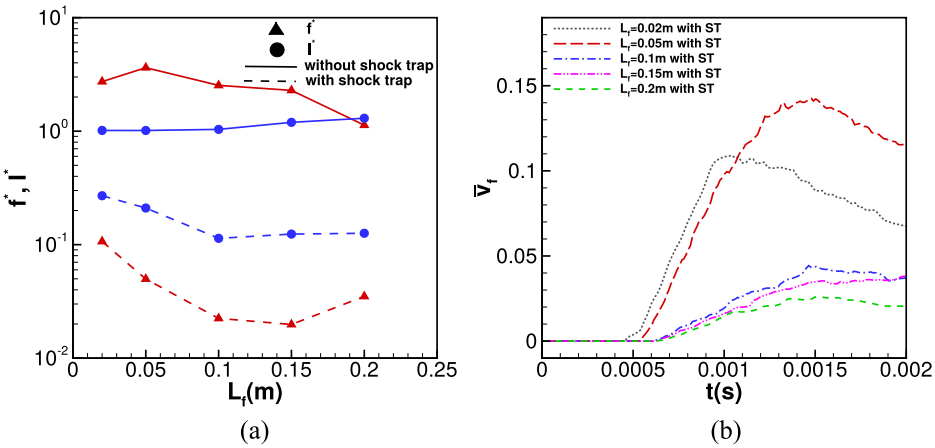

FIG. 17. Performance of the polystyrene foam-shock trap setup. (a) Comparison of the wall force and impulse values (non-dimensioned using the values of base case) for different foam thickness. (b) Temporal variation of volume of polystyrene foam exiting the shock trap.

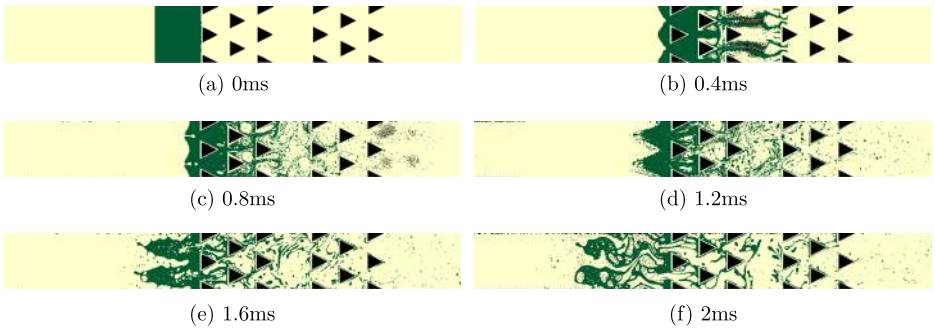

FIG. 18. Spatial distribution of air and polystyrene foam medium at various time instants for L_f = 0.1 m case. The colour code is yellow for air and green for polystyrene foam.

polystyrene foam barrier without the shock trap. It is observed that the shock amplification effect is relatively weaker in the case of aqueous foams. While the peak wall force for the aqueous foam is considerably lower than the polystyrene foam, the impulse transmitted is relatively higher. This is attributed to lower wave speed in the case of aqueous foam which leads

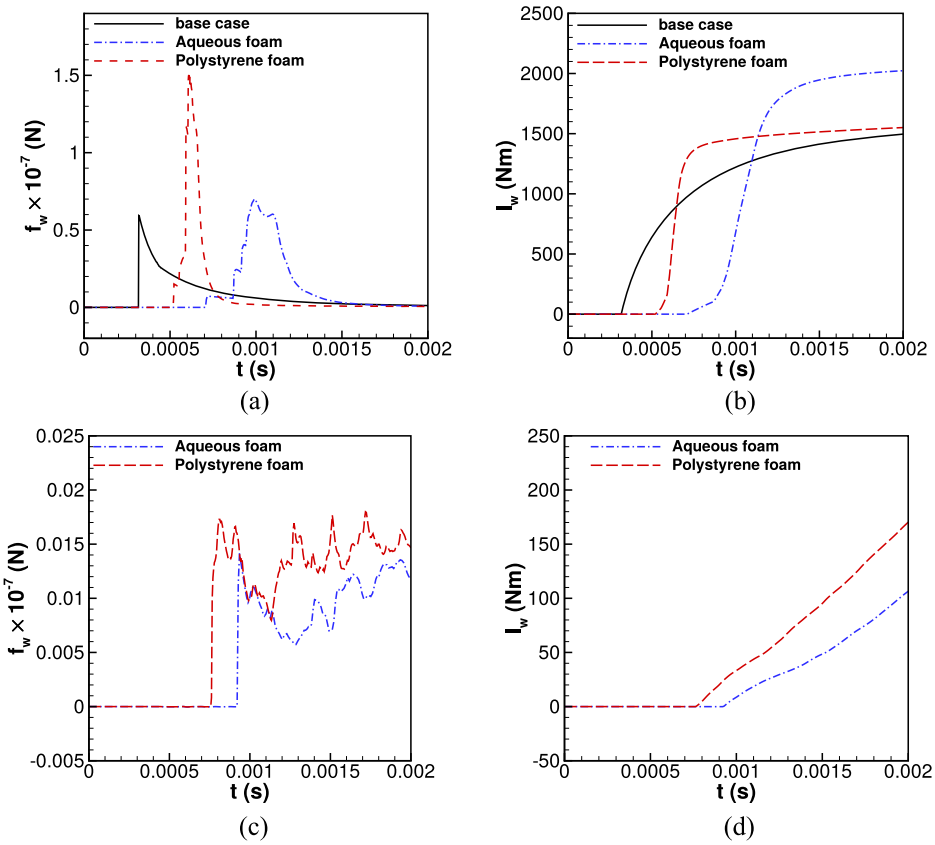

FIG. 19. Comparison of the (a) wall force and (b) impulse for aqueous foam and polystyrene foam barrier configuration without the shock trap. Comparison of (c) wall force and (d) impulse for the two different foams in combination with the shock trap. The results shown correspond to a foam thickness value of L_f = 0.1 m.

to a broadening of the loading history. Figures 19(c) and 19(d) compare the wall force and impulse obtained using aqueous and polystyrene foam barriers along with the shock trap. From the figures, it is observed that both foams exhibit good attenuation of the incident blast wave. It can be noticed that the loading characteristics are almost similar with only marginal differences. However, the aqueous foam shows slightly better mitigation of the blast. Since the blast attenuation of both foam materials is somewhat similar, it can be argued that the polystyrene foam-shock trap combination would be a better choice, particularly in the case on non-contact explosions. The ready availability, easier material handling, longer material degradation period, and good strength to weight ratio provide a clear advantage for the polystyrene foam over the aqueous foam, when employed in conjunction with the shock trap.

VI. SUMMARY AND CONCLUSIONS

In this work, blast mitigation characteristics of foams in combination with a special arrangement of rigid obstacles known as shock trap was presented. Detailed simulations were carried out using a hydrocode based on a mesh free, fully Lagrangian, particle based method called smoothed particle hydrodynamics. Two different foam materials were studied, namely, wet aqueous foam and polystyrene foam. A pseudo-gas approach with Nobel-Abel equation of state was used to model the aqueous foam. The polystyrene foam was modeled using a stiffened gas approach. The obstacle geometries which constitute the shock trap impose complicated wall boundary conditions within the flow domain. To efficiently handle these wall boundaries, a method based on skewed kernel functions called skew gradient wall boundary treatment was followed. A special SPH material interface treatment for accurately resolving the contact discontinuities was implemented. The incident blast wave was modeled using the Friedlander function with blast wave parameters corresponding to a strong blast condition.

From the simulations, it is found that the bulk motion of the foam material toward the target structure and subsequent compaction resulted in poor overall mitigation characteristics for foam barriers. With an increase in the foam thickness, the value of peak force exerted on the target structure was found to be drastically lower. For the same incident blast conditions, the aqueous foam barrier coupled with the shock trap has shown a 95% reduction in the peak force and 90% reduction in impulse. Considerable delay in the arrival of the blast wave and broadening of the loading history was also noticed.

Most importantly, the shock enhancement effect from foam was absent for all the cases that were studied. For higher values of foam thickness (beyond L_f = 0.1 m), the aqueous foam-shock trap setup has shown only marginal improvement in the mitigation of the blast load. With less than 10% of the initial volume of the aqueous foam exiting the shock trap, the proposed shock trap was found to be a very effective mechanism to avoid foam stagnation at the protected structure and the attendant amplification of the blast load. For the polystyrene foam-shock trap setup, the reduction in the value of peak force and the impulse was found to be greater than 93% and 79%, respectively. When compared to the polystyrene foam barrier approach, the proposed polystyrene foam-shock trap method has shown an order of magnitude reduction in the value of force and impulse exerted on the target structure. The amount of polystyrene foam exiting the shock trap was less than 15% of the initial foam volume for lower foam thickness and less than 5% for higher foam thickness. Both aqueous and polystyrene foam barriers in conjunction with the shock trap setup produced comparable results despite the large difference in the value of foam density. Although the aqueous foam-shock trap setup has shown relatively improved blast mitigation, it may be noted that the polystyrene foam-shock trap setup could be a better choice owing to the material degradation aspects associated with the aqueous foam.

ACKNOWLEDGMENTS

The financial support of Armament Research Board, DRDO, The Government of India, is gratefully acknowledged (Project No. ARMREB/CDSW/2015/165). The authors also thank the anonymous referees for their valuable suggestions.

[1]O. Igra, J. Falcovitz, L. Houas, and G. Jourdan, "Review of methods to attenuate shock/blast waves," Prog. Aerosp. Sci. **58**, 1–35 (2013).
[2]A. Britan, H. Shapiro, M. Liverts, G. Ben-Dor, A. Chinnayya, and A. Hadjadj, "Macro-mechanical modelling of blast wave mitigation in foams. Part I: Review of available experiments and models," Shock Waves **23**, 5–23 (2013).
[3]S. Sembian, M. Liverts, and N. Apazidis, "Attenuation of strong external blast by foam barriers," Phys. Fluids **28**, 096105 (2016).
[4]P. V. Komissarov, A. A. Borisov, G. N. Sokolov, and V. V. Lavrov, "Rigid polyurethane foam as an efficient material for shock wave attenuation," J. Phys.: Conf. Ser. **751**, 012020 (2016).
[5]I. S. Sandhu, A. Sharma, Prince, M. K. Singh, R. Kumari, P. S. Alegaonkar, and D. Saroha, "Study of blast wave pressure modification through rubber foam," Procedia Eng. **173**, 570–576 (2017).
[6]Y. Xia, C. Wu, Z.-X. Liu, and Y. Yuan, "Protective effect of graded density aluminium foam on RC slab under blast loading—An experimental study," Constr. Build. Mater. **111**, 209–222 (2016).
[7]B. Nie, L. Yang, and J. Wang, "Experiments and mechanisms of gas explosion suppression with foam ceramics," Combust. Sci. Technol. **188**, 2117–2127 (2016).
[8]X. Li, P. Zhang, Z. Wang, G. Wu, and L. Zhao, "Dynamic behavior of aluminum honeycomb sandwich panels under air blast: Experiment and numerical analysis," Compos. Struct. **108**, 1001–1008 (2014).
[9]G. Jourdan, C. Mariani, L. Houas, A. Chinnayya, A. Hadjadj, E. Del Prete, J.-F. Haas, N. Rambert, D. Counilh, and S. Faure, "Analysis of shock-wave propagation in aqueous foams using shock tube experiments," Phys. Fluids **27**, 056101 (2015).
[10]M. Liverts, O. Ram, O. Sadot, N. Apazidis, and G. Ben-Dor, "Mitigation of exploding-wire-generated blast-waves by aqueous foam," Phys. Fluids **27**, 076103 (2015).
[11]B. W. Skews, M. D. Atkins, and M. W. Seitz, "The impact of a shock wave on porous compressible foams," J. Fluid Mech. **253**, 245–265 (1993).
[12]O. E. Petel, S. Ouellet, A. J. Higgins, and D. L. Frost, "The elastic-plastic behaviour of foam under shock loading," Shock Waves **23**, 55–67 (2013).
[13]Y. Sugiyama, T. Homae, K. Wakabayashi, T. Matsumura, and Y. Nakayama, "Numerical simulations on the attenuation effect of a barrier material on a blast wave," J. Loss Prev. Process Ind. **32**, 135–143 (2014).
[14]F. Zhu, C. C. Chou, and K. H. Yang, "Shock enhancement effect of lightweight composite structures and materials," Composites, Part B **42**, 1202–1211 (2011).
[15]L. Chen, Q. Fang, L. Zhang, Y. Zhang, and W. Chen, "Numerical investigation of a water barrier against blast loadings," Eng. Struct. **111**, 199–216 (2016).
[16]R. Hajek, M. Foglar, and J. Fladr, "Influence of barrier material and barrier shape on blast wave mitigation," Constr. Build. Mater. **120**, 54–64 (2016).
[17]S. Seeraj and B. W. Skews, "Dual-element directional shock wave attenuators," Exp. Therm. Fluid Sci. **33**, 503–516 (2009).

[18]Y. Andreopoulos, S. Xanthos, and K. Subramaniam, "Moving shocks through metallic grids: Their interaction and potential for blast wave mitigation," Shock Waves **16**, 455–466 (2007).
[19]D. Igra and O. Igra, "Shock wave mitigation by different combination of plate barriers; a numerical investigation," Eur. J. Mech. B: Fluids **59**, 115–123 (2016).
[20]S. S. Prasanna Kumar, B. S. V. Patnaik, and K. Ramamurthi, "Prediction of air blast mitigation in an array of rigid obstacles using smoothed particle hydrodynamics," Phys. Fluids **30**, 046105 (2018).
[21]B. W. Skews, M. A. Draxl, L. Felthun, and M. W. Seitz, "Shock wave trapping," Shock Waves **8**, 23–28 (1998).
[22]A. Chaudhuri, A. Hadjadj, O. Sadot, and G. Ben-Dor, "Numerical study of shock-wave mitigation through matrices of solid obstacles," Shock Waves **23**, 91–101 (2013).
[23]J. J. Monaghan, "Smoothed particle hydrodynamics and its diverse applications," Annu. Rev. Fluid Mech. **44**, 323–346 (2012).
[24]G. R. Liu and M. B. Liu, *Smoothed Particle Hydrodynamics: A Meshfree Particle Method* (World Scientific, 2003).
[25]D. Price, "Smoothed particle hydrodynamics and magnetohydrodynamics," J. Comput. Phys. **231**, 759–794 (2012).
[26]D. Price, "Modelling discontinuities and Kelvin-Helmholtz instabilities in SPH," J. Comput. Phys. **227**, 10040–10057 (2008).
[27]W. Dehnen and H. Aly, "Improving convergence in smoothed particle hydrodynamics simulations without pairing instability," Mon. Not. R. Astron. Soc. **425**, 1068–1082 (2012).
[28]L. Cullen and W. Dehnen, "Inviscid smoothed particle hydrodynamics," Mon. Not. R. Astron. Soc. **408**, 669–683 (2010).
[29]Z.-Y. Liu, "Overdriven detonation phenomenon and its applications to ultra-high pressure generation," Ph.D. dissertation (Kumamoto University, 2001).
[30]S. S. Prasanna Kumar and B. S. V. Patnaik, "A multimass correction for multicomponent fluid flow simulation using smoothed particle hydrodynamics," Int. J. Numer. Methods Eng. **113**, 1929–1949 (2018).
[31]S. S. Prasanna Kumar, B. S. V. Patnaik, and G. R. Liu, "A skewed kernel approach for the simulation of shocks using SPH," Int. J. Numer. Methods Eng. **111**, 383–400 (2017).
[32]H. Wendland, "Piecewise polynomial, positive definite and compactly supported radial functions of minimal degree," Adv. Comput. Math. **4**, 389–396 (1995).
[33]S. Rosswog, "Boosting the accuracy of SPH techniques: Newtonian and special-relativistic tests," Mon. Not. R. Astron. Soc. **448**, 3628–3664 (2015).
[34]T. Homae, K. Wakabayashi, T. Matsumura, and Y. Nakayama, "Attenuation of blast wave using water gel," Sci. Technol. Energ. Mater. **67**, 182–186 (2006).
[35]L. Brookshaw, "Smooth particle hydrodynamics in cylindrical coordinates," ANZIAM J. **44**(E), C114–C139 (2003).
[36]D. Garcia-Senz, A. Relano, R. M. Cabezon, and E. Bravo, "Axisymmetric smoothed particle hydrodynamics with self-gravity," Mon. Not. R. Astron. Soc. **392**, 346–360 (2009).
[37]C. N. Kingery and G. Bulmash, "Airblast parameters from TNT spherical air burst and hemispherical surface burst," Technical Report ARBRL-TR-02555, Ballistics Research Laboratory, 2006.
[38]D. Hui and P. K. Dutta, "A new concept of shock mitigation by impedance-graded materials," Composites, Part B **42**, 2181–2184 (2011).
[39]M. Liang, Z. Li, F. Lu, and X. Li, "Theoretical and numerical investigation of blast responses of continuous-density graded cellular materials," Compos. Struct. **164**, 170–179 (2017).
[40]K. Kitagawa, M. Yasuhara, and K. Takayama, "Attenuation of shock waves propagating in polyurethane foams," Shock Waves **15**, 437–445 (2006).
[41]D. Reese and C. Weber, "Numerical investigation of 3D effects on a 2D-dominated shocked mixing layer," Phys. Fluids **28**, 114102 (2016).
[42]S. Sembian, M. Liverts, N. Tillmark, and N. Apazidis, "Plane shock wave interaction with a cylindrical water column," Phys. Fluids **28**, 056102 (2016).
[43]Y. Liang, J. Ding, Z. Zhai, T. Si, and X. Luo, "Interaction of cylindrically converging diffracted shock with uniform interface," Phys. Fluids **29**, 086101 (2017).
[44]W. Peng, Z. Zhang, G. Gogos, and G. Gazonas, "Fluid structure interactions for blast wave mitigation," J. Appl. Mech. **78**, 031016-1–031016-8 (2011).
[45]R. Höhler and S. Cohen-Addad, "Rheology of liquid foam," J. Phys.: Condens. Matter **17**, R1041 (2005).
[46]A. Britan, G. Ben-Dor, H. Shapiro, M. Liverts, and I. Shreiber, "Drainage effects on shock wave propagating through aqueous foams," Colloids Surf., A **309**, 137–150 (2007).